Research Article Vol. 14, No. 6 / 1 Jun 2023 / Biomedical Optics Express 3003
Biomedical Optics EXPRESS

On-chip clearing for live imaging of 3D cell cultures

TINGTING YU,[1,2,†] XIANG ZHONG,[1,2,†] QIHANG YANG,[1,2] CHAO GAO,[1,2] WENYUE CHEN,[1,2] XIANG LIU,[1,2] ZHANG LIU,[1,2] TINGTING ZHU,[2,3] DONGYU LI,[2,3] PENG FEI,[2,3] ZAOZAO CHEN,[4,5] ZHONGZE GU,[4,5] AND DAN ZHU[1,2,*]

[1]*Britton Chance Center for Biomedical Photonics - MoE Key Laboratory for Biomedical Photonics, Huazhong University of Science and Technology, Wuhan, Hubei 430074, China*
[2]*Wuhan National Laboratory for Optoelectronics - Advanced Biomedical Imaging Facility, Huazhong University of Science and Technology, Wuhan, Hubei 430074, China*
[3]*School of Optical and Electronic Information, Huazhong University of Science and Technology, Wuhan, Hubei 430074, China*
[4]*State Key Laboratory of Bioelectronics, School of Biological Science and Medical Engineering, Southeast University, Nanjing, Jiangsu 210096, China*
[5]*Institute of Biomaterials and Medical Devices, Southeast University, Suzhou, Jiangsu, 215163, China*
[†]These authors contributed equally to this work.
[*]*dawnzh@mail.hust.edu.cn*

Abstract: Three-dimensional (3D) cell cultures provide an important model for various biological studies by bridging the gap between two-dimensional (2D) cell cultures and animal tissues. Microfluidics has recently provided controllable platforms for handling and analyzing 3D cell cultures. However, on-chip imaging of 3D cell cultures within microfluidic devices is hindered by the inherent high scattering of 3D tissues. Tissue optical clearing techniques have been used to address this concern but remain limited to fixed samples. As such, there is still a need for an on-chip clearing method for imaging live 3D cell cultures. Here, to achieve on-chip clearing for live imaging of 3D cell cultures, we conceived a simple microfluidic device by integrating a U-shaped concave for culture, parallel channels with micropillars, and differentiated surface treatment to enable on-chip 3D cell culture, clearing, and live imaging with minimal disturbance. The on-chip tissue clearing increased the imaging performance of live 3D spheroids with no influence on cell viability or spheroid proliferation and demonstrated robust compatibility with several commonly used cell probes. It allowed dynamic tracking of lysosomes in live tumor spheroids and enabled quantitative analysis of their motility in the deeper layer. Our proposed method of on-chip clearing for live imaging of 3D cell cultures provides an alternative for dynamic monitoring of deep tissue on a microfluidic device and has the potential to be used in 3D culture-based assays for high-throughput applications.

1. Introduction

Three-dimensional (3D) cell cultures, such as spheroids and organoids, bridge the gap between two-dimensional (2D) cultures and *in vivo* tissues in animals [1]. 3D cultures can emulate physiological cell-cell and cell-extracellular matrix (ECM) interactions, better mimic *in vivo* tissues with closer architecture and greater physiological relevance than conventional 2D cultures, and decrease the cost and ethical issues associated with the usage of experimental animals [2]. 3D cultures have provided important models for a broad range of biological studies ranging from organogenesis, tissue engineering, tumor biology, drug screening, and many other biomedical applications [3–7]. In the past decade, advances in microfluidics have contributed significantly to the development of 3D cultures [8–11]. Spheroids or organoids have been combined with

#489219 https://doi.org/10.1364/BOE.489219
Journal © 2023 Received 10 Mar 2023; revised 7 May 2023; accepted 7 May 2023; published 31 May 2023

Biomedical Optics EXPRESS

microfluidic technology to create organ-on-a-chip systems, where microfluidic technology is exploited to actively control flow conditions, mechanical stressors, and the chemical environment [12]. Multiple studies have shown that spheroids cultured on microfluidic chips can better recapitulate the *in vivo* microenvironment [13].

To fully exploit the benefits of on-chip 3D cell cultures, 3D visualization is crucial. Modern optical imaging techniques provide powerful tools to observe thick tissues in 3D with high resolution; however, imaging is highly limited due to multilayered cells and thickness, which limits light penetration leading to unsatisfactory imaging performance in deeper tissue layers [14]. Moreover, chip systems often introduce extra limitations for imaging depth due to complicated fabrications [15]. Tissue optical clearing technology reduces light attentuation and improves penetration depth by matching the refractive index between components via kinds of physical and chemical strategies [16–18].

Tissue optical clearing techniques can render real tissues and even whole animal bodies transparent [18–23]. In recent years, multiple optimized clearing protocols have been proposed for 3D culture models [24–26], such as brain organoids [26–28], stem cell spheres [29], human dermal fibroblasts (HFIB) spheroids [30,31], intestinal organoids [32], tumor spheroids [33], which permitted high-depth imaging of these models. Most of these clearing protocols require repeated solution exchange, which is labor-intensive, difficult to implement for small 3D cell cultures, and prone to sample loss or damage. It is also hard to track the same 3D cell cultures throughout the entire experimental process [34]. Considering the ease of handling and high throughput, several groups have engineered microfluidic platforms for on-chip clearing of 3D cell cultures [12,34–37]. Still, these protocols remain limited to fixed samples due to the use of harsh mounting conditions or toxic chemicals [24], which are incapable of dynamic monitoring of growth, development, and pathological reactions in 3D cell cultures. Hence, there is a need for effective, microfluidic-based tissue clearing platforms for imaging live 3D cell cultures.

In this study, we described the on-chip clearing for live imaging of 3D cell cultures. We first fabricated an integrated microfluidic device for 3D culture, clearing, and live imaging on-chip. We then developed an on-chip tissue clearing protocol based on iodixanol for live 3D cell cultures, and further evaluated imaging performance in tumor spheroids. Furthermore, we applied the on-chip tissue clearing to monitor the motility of lysosomes in live tumor spheroids.

2. Methods

2.1. Microfluidic chip design

The device consists of four parts: a top layer with a cover glass and two in/outlets, a punched polydimethylsiloxane (PDMS) membrane, a patterned PDMS layer, and a bottom layer with a glass slide. The patterned PDMS layer contains three microfluidic units, and each unit includes two parallel channels: a culture channel and a clearing channel. Seven U-shaped concave chambers, each about 2 mm in diameter, were equally spaced under the culture channel with an interval of 3.5 mm. The width of the culture channel and clearing channel were 600 µm and 1000 µm, respectively, with the same length of 3.5 cm. The joints of the two channels were 1000 µm in width, including two micropillars 200 µm in width served as a buffer to reduce the impact of the fluid on the spheroids.

2.2. Microfluidic chip fabrication

2.2.1. Soft lithography

The silicon mold was made with soft lithography according to the following procedure: the wafer was uniformly coated with SU-8 2150 negative photoresist (Microchem, USA) using a spinner, then baked at 65°C for 5 min and then 95°C for 30 min. After selective exposure through a film

Biomedical Optics EXPRESS

photomask with an energy dose of 260 mJ/cm^2, the wafer was further baked at 65°C for 5 min, then 95°C for 12 min. After development, the wafer was cleaned for subsequent experiments.

2.2.2. Patterned PDMS layer fabrication

The PDMS prepolymer was produced by mixing PDMS (Sylgard 184, Dow Corning, USA) with curing agent at a 10:1 ratio (by weight). After vacuum treating for 1 h at room temperature (RT), 13.5 g of PDMS prepolymer was poured on the silicon mold and placed in 80°C oven for 1 h for solidification. Then, the solid PDMS was carefully peeled off the mold and wells were created with a biopsy punch. Next, the patterned PDMS layer and glass slide were cleaned with residue-free tape and an ultrasonic cleaning machine for 30 min, treated with oxygen plasma for 100 s to form covalent bonding, and then kept at 80 °C for at least 1 h to enhance the bonding effect.

2.2.3. U-shaped bottom fabrication

PDMS prepolymer was loaded into a syringe with a 0.6 mm needle, and the gas in the syringe was discharged. Next, the syringe was continuously and slowly pushed and the PDMS droplets were added to wells that were formed by the punched PDMS layer and the cover glass (Fig.S1). The device was then placed under a vacuum for 30 min, followed by 80°C incubation for 3 h to form the solidified U-shaped bottom.

2.2.4. Surface treatment

A differentiated surface treatment between the cover glass and the U-shaped bottom was created. Prior to bonding, the cover glass of the top layer was treated with L-Polylysine for 30 min to form an adherent surface for anchoring the tumor spheroids. After bonding, the channels were infused with the Anti-adherence agent (StemCell, Canada) until filled; then, the device was placed under gnotobasis for 30 min to form a low adherent surface at the U-shaped bottom and subsequently reinfused with deionized water followed by nitrogen. A vacuum was then applied for 6 h at RT to remove the bubbles.

2.3. Fluid dynamics simulation

Finite element simulations at different perfusion velocities during clearing were performed by COMSOL Multiphysics 6.1 (COMSOL, USA). Multi-physical field simulation was carried out using laminar flow and transport of dilute species to simulate the diffusion process of the reagent. The shear rate and pressure drop were recorded. Further, to find an appropriate perfusion velocity for clearing protocol, perfusion velocity ranges from 0.6 µL/min to 600 µL/min were applied with the viscosity of iodixanol acquired with an NDJ-1F viscosimeter (QIGAO, China). After the uniform diffusion of iodixanol in the culture channel, the levels of pressure, velocity magnitude, and shear stress in the channel under different perfusion velocities and chip designs were compared and evaluated.

2.4. Spheroid formation on the microfluidic chip

MCF-7 cell line that expresses GFP endogenously (a gift from Prof. Yiwei Li's lab, China) and human umbilical vein endothelial cells (HUVEC) cell line (ScienceCell, USA) were used in this study. MCF-7 cells and HUVEC cells were grown in Dulbecco's modified eagle medium (DMEM) and endothelial cell medium (ECM), respectively, which were both supplemented with 10% fetal bovine serum (FBS) and 1% penicillin-streptomycin. Once the cells had grown to 80–90% confluence, they were harvested by 0.25% Trypsin-EDTA treatment and resuspended in the complete medium to a suspension volume of 1×10^6 cells/mL.

Then, the MCF-7 cell suspension was infused into the culture channel with the clearing channel locked. Once the culture channel was filled, the device was centrifuged at 400 g for 5 min, and

Biomedical Optics EXPRESS

reinfused at 2 μL/min with DMEM to remove the residual cells outside the culture chambers, followed by re-centrifugation at 100 g for 5 min.

The cells were cultured in a humidified incubator (Thermo Fisher Scientific, USA) maintained at 37°C and 5% CO_2. The device was perfused with culture medium every 24 h, and a syringe filled with the medium was linked to each channel of the device.

For the co-culture spheroid formation, suspensions of MCF-7 and HUVEC cells were mixed at a volume ratio of 3:1, then infused and cultured using the same protocol as above.

2.5. Staining

The working solutions of five chemical dyes were prepared according to the standard protocols, including propidium iodide (PI) (C2015M, beyotime, China), Calcein-AM (C2015M, beyotime, China), Hoechst 33342 (C1027, beyotime, China), Annexin-V (40304ES20, Yeasen, China), and LysoTracker Red (C1046, beyotime, China). The dilutions of the dyes are as follows, 1:1000 for PI and Calcein-AM, 1:100 for Hoechst 33342, 1:50 for Annexin-V, and 1:20000 for LysoTracker Red.

Prior to staining, the tumor spheroids were perfused with PBS at 18 μL/min for 10 min to remove the metabolic waste. Next, the working solutions were perfused at 18 μL/min for the following time spans: 20 min for PI, Hoechst 33342, Annexin-V, and Calcein-AM, 40 min for LysoTracker Red. The device was then reinfused with culture medium for 10 min to remove the residual dye.

2.6. Clearing

2.6.1. Preparation of agents

The solutions were prepared by mixing glycerol (V900122, Vetec, USA), iohexol (I134719, Aladdin, China), and iodixanol (D1556, Sigma-Aldrich, USA) with the complete medium or deionized water at different ratios. The transmittance was measured with a spectrophotometer (Lambda 950, PerkinElmer, USA). The Osmotic pressure was measured using a Gonotec-3000 osmometer (Gonotec, Germany). The refractive indices were measured at 20°C using an Abbe refractometer (WAY-2S, Shanghai YiCe Apparatus & Equipment Co., Ltd., Shanghai, China) at 589 nm.

2.6.2. On-chip clearing

After infusion of culture medium to remove metabolic waste, the clearing channels were infused with the 20% (v/v) iodixanol solution at 18 μL/min for about 10 min. The spheroids were recovered by reinfusing the culture medium.

2.7. Cell viability test

Cell viability was assessed using Cell Counting Kit-8 (CCK-8) (40203ES76, Yeason, China), which was based on WST-8, a tetrazolium salt reduced by dehydrogenases to a yellow dye detected at 450 nm. The device was first perfused with medium at 18 μL/min for 10 min. After that, the CCK-8 working solution was introduced into the channel at 18 μL/min for 10 min to fulfill the culture chamber. Then, the spheroids were incubated for an hour with a continuous flow at 2 μL/min. The waste collected by a centrifuge tube was analyzed by a Microplate Reader (BioTek, USA).

2.8. Imaging

Images of the chip were acquired with a Panasonic DC-GX9 camera, and enlarged details were obtained under a Motic DM-143-FBLED-A5 microscope. The bright-field images of the tumor spheroids were acquired with an IX70 Fluorescence microscope (Olympus, Japan), and the

Biomedical Optics EXPRESS

wide-field fluorescent images of spheroids were obtained with the Axio Zoom.V16 microscope (Zeiss, Germany). Confocal images and differential interference contrast (DIC) images were acquired with LSM710 confocal microscope (Zeiss, Germany) equipped with a Zeiss 10× Fluar objective (N.A., 0.5; air) and a Zeiss 40× Plan-Apochromat objective (N.A.,1.4; oil). The images before and after clearing were acquired with the same imaging parameters, and no z-axis laser intensity correction was applied.

2.9. Data analysis

The obtained images were analyzed with Fiji and MATLAB (MathWorks, USA). The 'brightness/contrast' in Fiji was used to adjust the images for better visualization. The DIC images were quantitated with Fiji's 'Plot profile'. In detail, pixel values reflecting the local optical path difference were acquired from a straight line perpendicular to the cytomembrane, and the refractive index difference was calculated by the ratio of the pixel values inside and outside the cytomembrane. The orthogonal view (x-z) of the image stacks was made with Fiji. To analyze lysosome motility, images were initially denoised by block-matching and 3D filtering (BM3D) method [38]. Fiji's implemented 'trackmate' was applied to trace the movement of lysosomes for both the no-clearing and the clearing groups, LoG detector and simple LAP tracker were applied; only tracks longer than 20 flames (20s) were analyzed. Imaris (Oxford Ins., UK) was applied for cell counting.

Statistical analyses were performed using GraphPad Prism 8 (GraphPad Software, USA). All numerical data are presented as mean ± standard deviation (S.D.). Unpaired t-test was used for pairwise comparison, one-way analysis of variance (ANOVA) was used for lysosome analyses and statistical significance was determined at $p < 0.05$.

3. Results

3.1. Design and fabrication of a microfluidic chip integrating 3D culture, live clearing and imaging

Mismatch of refractive indices between cultured samples, the culture media and chip functional elements are common obstacles in the imaging and analysis of 3D cell cultures on chip platforms. Tissue optical clearing techniques have been combined with microfluidic platforms to allow high-throughput structural analysis of 3D cell cultures but are limited to fixed samples. Here, we aimed to clear live 3D cell cultures on a microfluidic device to permit live imaging in deep tissue layers. To this goal, we conceived a microfluidic chip integrating 3D culture, tissue clearing, and live imaging. It consisted of a bottom support with a glass slide, a patterned PDMS layer for containing the channels, a punched PDMS membrane for sealing the chip and facilitating the liquid flow in the channels, a cover glass as the top layer for imaging, and the in/outlets. The device design and fabrication are shown in Fig. 1.

For spheroid culture, we utilized a U-shaped concave bottom which could be formed spontaneously under the surface tension of liquids (Fig. S1) and designed the culture chamber to be millimeter-scale both in width and depth to allow the formation of 3D spheroids with a necrotic core and a gradient of nutrients to mimic physiological conditions.

To reduce the disturbance to live spheroids during on-chip clearing, we introduced parallel channels and micropillars at the junction of the two channels. As shown in Fig. 1(a), the culture and clearing were overtaken by two independent channels and micropillars in-between to avoid direct infusion of the fluid. The simulation results of the relevant fluid parameters along the channels demonstrated that the parallel design could notably reduce the influence of direct perfusion (Fig. 1(b) & Fig. S2). Figure 1(c) shows a fabricated chip and locally enlarged images of the details from the top and side view.

Biomedical Optics EXPRESS

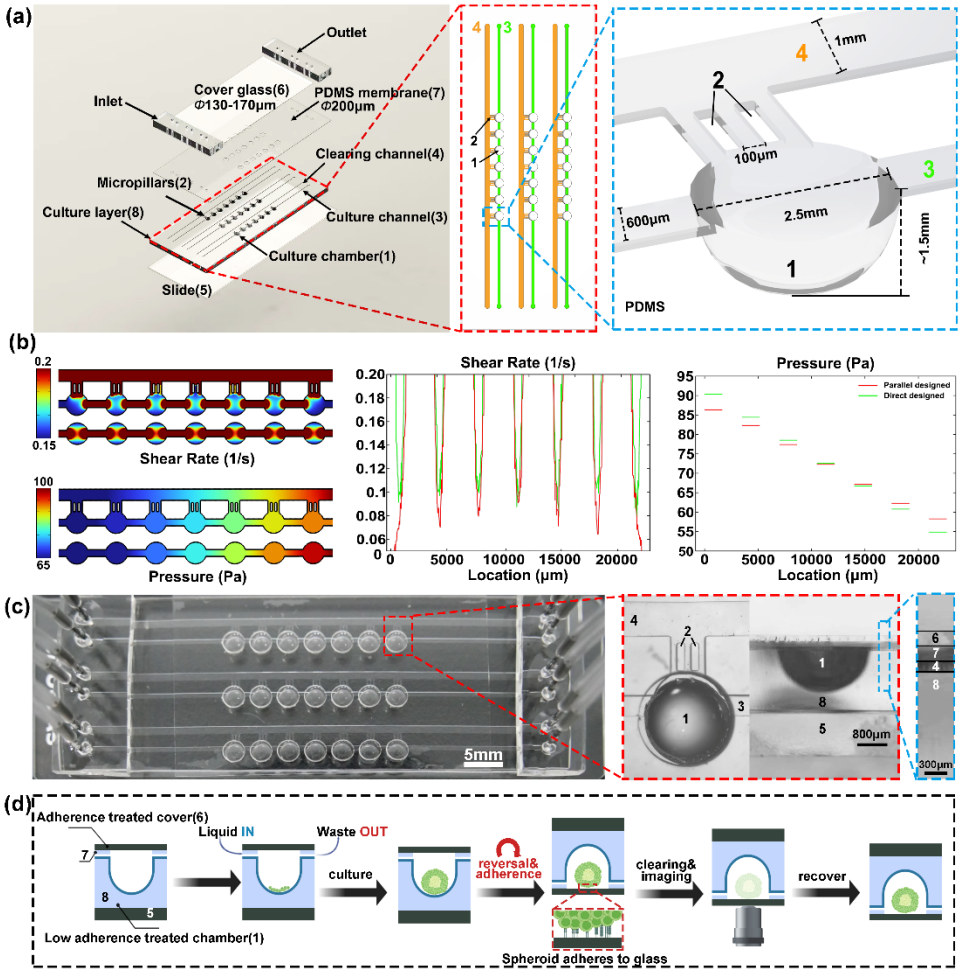

Fig. 1. Design and fabrication of the microfluidic chip for 3D culture, live clearing and imaging. (a) Schematic view of the chip with four layers including a bottom support with a glass slide, a patterned PDMS layer, a punched PDMS membrane and a top layer with a cover glass and in/outlets. The width of culture channel and clearing channel is approximately 600 μm and 1 mm, respectively. The diameter of the cylindrical well is about 2 mm and the depth of the U-shaped concave bottom is about 1.5 mm. (b) The parallel channels and micropillars reduce the disturbance. (c) Photograph of an actual chip device viewed from above and the enlarged images from the top view and side view. (d) Illustration of the pipeline of spheroid culture, clearing and imaging on the chip. 1: culture chamber; 2: micropillars; 3: culture channel; 4: clearing channel; 5: slide glass; 6: cover glass; 7: punched PDMS membrane; 8: culture layer.

For imaging, to bypass the refractive index (RI) mismatch of device material as far as possible, we punched the PDMS membrane to match with the concaved PDMS chamber, and covered the chip with a thin cover glass, which functioned as the imaging window. Here, we conceived a differentiated surface treatment between the cover glass and U-shaped bottom by considering the limited working distance of objectives. Unlike the low adherence treatment to the U-shaped bottom, we applied the adherence treatment to the cover glass to produce a surface with a certain degree of adherence capability so that the formed spheroids could be anchored by reversing

Biomedical Optics EXPRESS

the chip, permitting imaging with high-magnification objectives. Moreover, this reversal and adherence could hold the spheroids during infusion of clearing solution and repeated imaging to avoid floating and rotating, enabling continuous monitoring of the same region of the same spheroid, as shown in Fig. 1(d).

With this device, multiple MCF-7 spheroids were generated (Fig. S3). The cells aggregated after centrifugation (day 0), indicating the formation of cell-cell interactions, and the spheroids gradually increased to about 0.35 ± 0.06 mm^2 in the area during a 4-day culture. The above results demonstrated that this device enables multiple tumor spheroids production, which assured the feasibility of further investigation of the on-chip clearing and imaging.

3.2. Development of the microfluidic-based clearing protocol for live 3D cell cultures

To clear live 3D cell cultures, we first searched for effective clearing agents from compounds that combine high transmittance, high water solubility, dilution-dependent RI tuning, and low toxicity as crucial requirements for live-imaging compatibility. Three agents were considered, including glycerol, a commonly used clearing agent in skin, iohexol and iodixanol, two intravenous X-ray contrast agents widely used in clinical practice. The physicochemical properties of these agents are shown in Fig. S4. Iodixanol demonstrates great potential since it is optically transparent, displays a high RI, and, most importantly, is almost nearly isotonic to the cell culture media.

Since the RI of the spheroid sample was unknown, iodixanol concentration titration was performed. We incubated the cells in various concentrations of iodixanol and observed them with DIC microscopy. A loss of contrast between the sample and medium results from a match of RI. As shown in the DIC images and quantitative results, concentrations in the range of 15–25% would be appropriate clearing agents (Fig. 2(a)-(b)).

Next, to determine the infusion parameters for on-chip clearing, we built a finite element model of the microfluidic platform and simulated the fluid dynamics of the clearing agents with different flow rates ranging from 0.6 μL/min to 600 μL/min (Fig. 2(c)-(d)). The results showed that flow rates ranging from 4 μL/min to 44 μL/min allowed effective infusion of the agent to seven chambers in a reasonable time with shear stress close to physiological condition (0.1–1 dyn/cm^2). With a flow rate of 18 μL/min, the clearing agent filled the chambers in about 5 min. Further, we verified the clearing effect on MCF-7 spheroids by infusing 20% iodixanol solution at a rate of 18 μL/min on the microfluidic platform. The bright-field images of the same spheroid during clearing were recorded (Fig. 2(e), see Visualization 1), showing that the transparency of the spheroid was slightly enhanced, and did not notably change after 5 min (Fig. 2(f)). To ensure that the agent exchange was complete, and the tissue transparency reached the plateau, we determined 10 min as the optimal infusion time for the clearing protocol.

As toxicity is an important consideration in live imaging applications, we analyzed the safety of the clearing protocol for the spheroids from several aspects in view of cell viability and proliferation. The bright-field images and size measurement show that the clearing process did not change spheroid size during clearing (see Visualization 1). Next, we assessed the viability of 3D cell cultures using CCK-8. The results indicated that cell viability after on-chip clearing was comparable to the no-clearing group (Fig. 2(g)), and this viability was sustained for a minimum of two hours (Fig. S5). These findings suggest that the clearing method has no significant impact on cell viability. In addition, we compared the proliferation of 3D spheroids by monitoring their size at different time points. As shown in Fig. 2(h), there is no significant difference between the size of spheroids with and without clearing. These results indicated that the clearing protocol has no obvious harmful effects on cell viability and spheroid proliferation.

3.3. Increased imaging performance by on-chip tissue clearing

To assess the improvement of on-chip clearing on imaging performance, we applied the clearing protocol to MCF-7 tumor spheroids and performed confocal microscopy.

Biomedical Optics EXPRESS

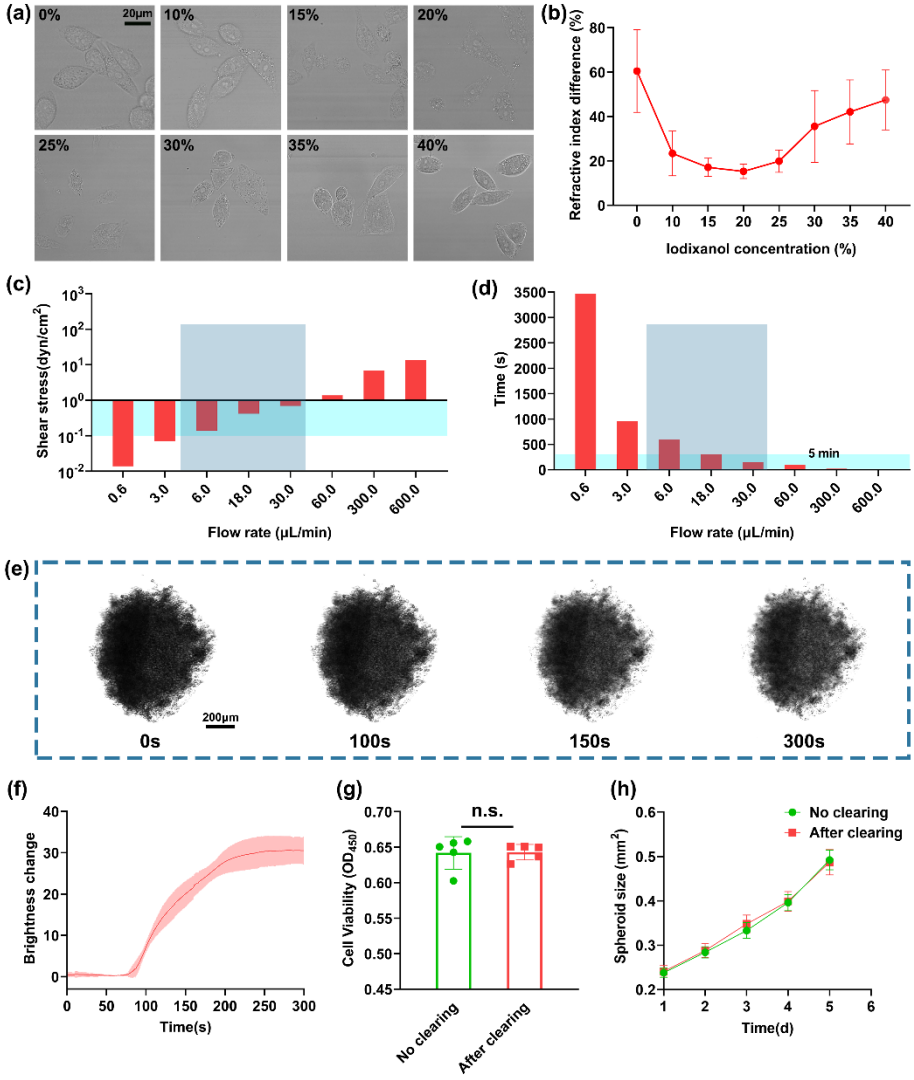

Fig. 2. Iodixanol-based on-chip clearing for live spheroids (a) DIC images of iodixanol-treated MCF-7 cells. (b) Quantification of the refractive index matching degree. (c)-(d) Comparison of shear stress and agent exchange time under different flow rates via fluid dynamics simulation. (e) Bright-field images of the same MCF-7 tumor spheroid during clearing. (f) The brightness curve of the spheroid along with time. (g)-(h) Safety assessment of the clearing protocol by comparing the cell viability and spheroid proliferation. The values are the mean ± S.D.; statistical significance (n.s., not significant) was assessed by unpaired t test.

First, we investigated the fluorescence compatibility of the clearing solution with both endogenous GFP and exogenous fluorescent probes, including PI, Hoechst 33342, Calcein-AM, and Annexin-V, which are commonly used chemical dyes for live and dead cell staining. The iodixanol-based clearing agent showed robust compatibility with the above fluorescent probes (Fig. S6), which allows for multi-color imaging.

Biomedical Optics EXPRESS

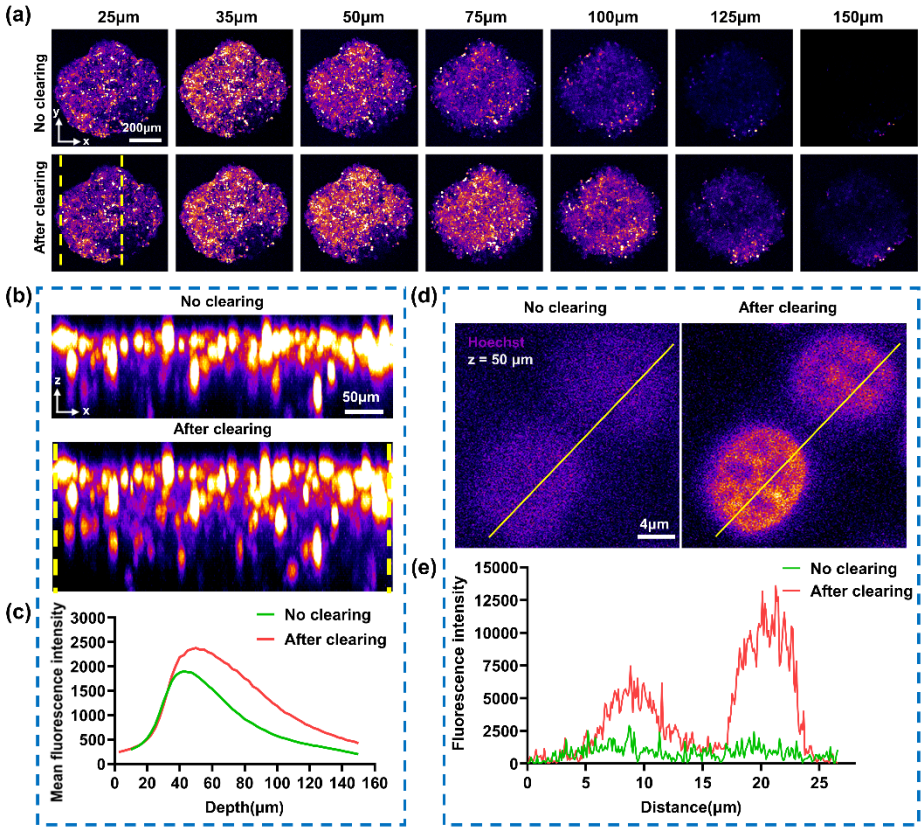

Fig. 3. Increased imaging performance after on-chip clearing. (a) Fluorescence images of MCF-7 tumor spheroid at different depths before and after clearing. (b) Orthogonal view (x-z) of the region indicated by the dashed yellow lines in (a). (c) Represented curves of fluorescence intensity against z depth. (d) High-magnification images of cells in spheroid at a depth of 50 μm before and after clearing. (e)The plot of signal intensity along the yellow lines in the images in (d).

Then, we imaged the same spheroid in the same region before and after clearing. The images at different depths are demonstrated in Fig. 3(a). The results showed that on-chip clearing effectively increased the GFP fluorescence intensity in deeper layers, and significantly improved cell counting (Fig. S7). Based on the obtained image stacks, we made an orthogonal projection (x–z projection) and plotted the fluorescence intensity curves against the z depth (Fig. 3(b)-(c)). The calculation showed that the clearing protocol increased the image depth by about 30%.

Further, to test the increased performance at high magnification, we stained the MCF-7 spheroids with Hoechst 33342 and observed the nucleus with a 40× oil objective before and after clearing at the same depth with the same imaging parameters. As shown in Fig. 3(d)-(e), the cell nucleus signal at a depth of 50 μm is hard to detect before clearing, while clearing substantially increased the imaging quality, enabling detection and distinguishment of the cell nucleus at a deeper layer.

3.4. On-chip clearing permits the monitoring of lysosomes in deeper layers

To demonstrate the biological application of on-chip clearing for live spheroids, we targeted the intracellular movement of organelles, which is fundamental to multicellular systems. The

Biomedical Optics EXPRESS

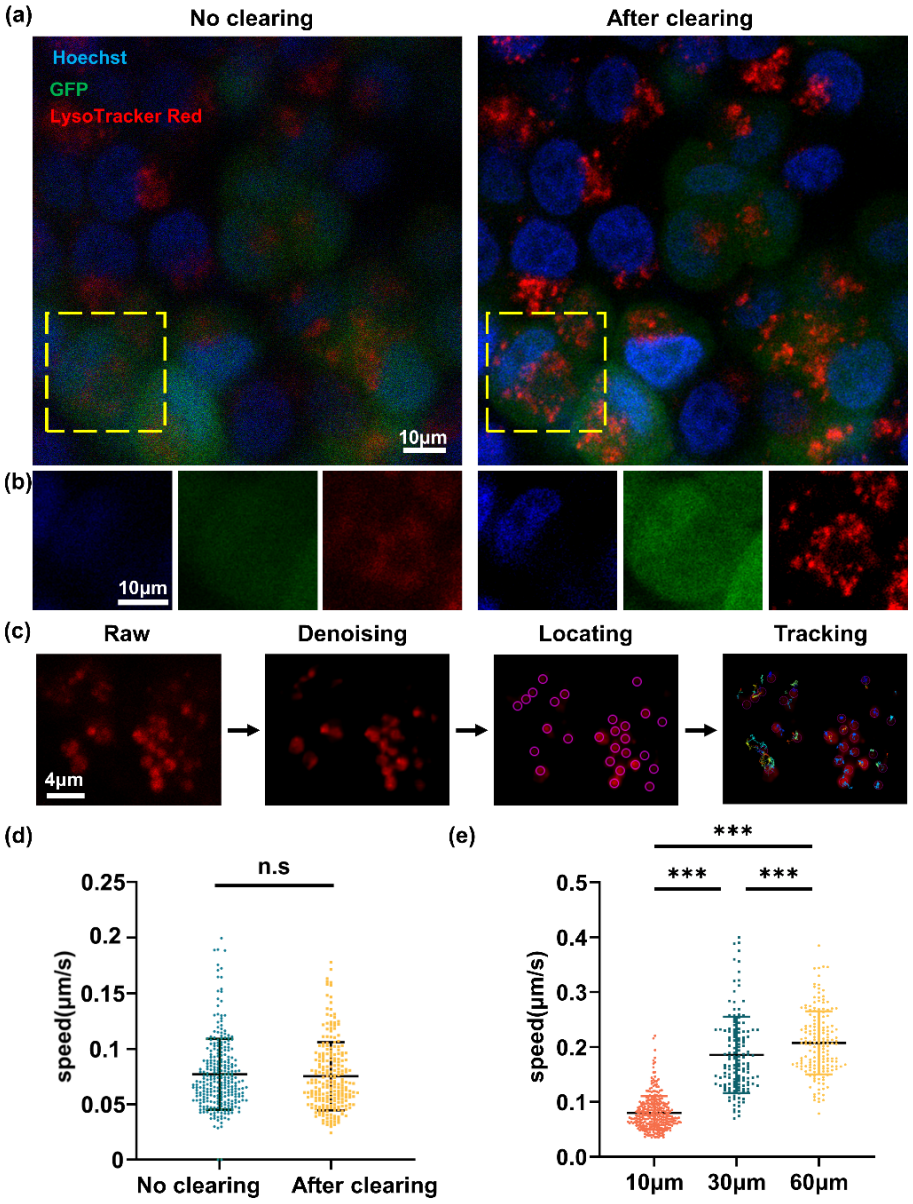

Fig. 4. Monitoring and analysis of lysosome motility in the spheroids. (a) The confocal images of the same spheroid at a depth of 60 μm before and after clearing. Red, LysoTracker red; green, GFP; blue, Hoechst 33342. (b) The enlarged views of the dashed boxed regions in (a). (c) The pipeline for image processing and tracking of lysosomes. (d) Comparison of movement speed before and after clearing at a superficial depth. (e) Quantification of lysosome movement speed at different depths. The values are the mean ± S.D.; statistical significance (n.s., not significant; *, $p < 0.05$; ***, $p < 0.001$) was assessed by unpaired t test in Fig. 4(d) and by one-way ANOVA in Fig. 4(e).

motility of lysosomes is closely related to cancer development and progression. Here, we tried to monitor lysosome movement in a co-culture spheroid of MCF-7 cells and endothelial cells. The multi-color images of the spheroid at a depth of 60 μm are shown in Fig. 4(a)-(b).

Biomedical Optics EXPRESS

Comparison between the no-clearing and clearing groups further showed the improvement of imaging performance by on-chip clearing

We tracked and quantified the trajectories of the lysosomes to characterize their motility (see Visualization 2). Figure 4(c) illustrates the image processing pipeline for tracking lysosomes. As shown in Fig. 4(d), the movement of lysosomes after clearing shows no significant difference from the initial state in the superficial layer, suggesting that the clearing process did not affect the lysosome motility, reinforcing the safety of the clearing protocol. In addition, the counting and tracking of lysosomes at deeper layers also indicate the effectiveness of the clearing method, as demonstrated in Fig. S8 and Fig. S9.

Then, with the aid of clearing, we monitored the dynamic movement of lysosomes in live spheroids at different depths in the co-culture spheroids, the results showed that the moving speed gradually increased with depth significantly, indicating more active lysosome motility at inner layers (Fig. 4(e)). This difference could hardly be observed without clearing, because the identification and tracking of lysosomes was extremely difficult before clearing.

4. Discussion

In this study, we introduced an on-chip clearing method for live imaging of 3D cell cultures based on a microfluidic device, which integrated 3D culture, clearing, and imaging. We utilized the U-shaped concave bottom for 3D culture, designed the parallel culture and clearing channels with micropillars for minimal disturbance, and combined the differentiated surface treatment for subsequent imaging. Iodixanol-based on-chip clearing increased the signal intensity and the imaging depth of 3D cell cultures and demonstrated robust compatibility with several commonly-used fluorescent probes, with no harmful effects on cell viability or spheroid proliferation. Our method permitted monitoring of the dynamic movement of organelles in deeper 3D cell cultures.

Besides the numerous tissue clearing protocols for fixed tissues, multiple studies have focused on *in vivo* clearing methods for animal tissues for live imaging, mainly for the skin and skull [39–43]. The commonly used *in vivo* clearing agents include sugars, sugar-alcohols and detergents, which are generally in high concentration and high osmolarity, making them inapplicable with live cellular models. Iodixanol has previously been applied for refractive index matching medium for live tissues [44], which inspired us to combine it with the microfluidic device for on-chip clearing and imaging of spheroids. Very recently, 60% iodixanol has been used to clear ligamentum flavum to establish an optically cleared intervertebral window for *in vivo* imaging of the mouse spinal cord [45]. In our study, we introduced iodixanol into on-chip clearing to enhance imaging performance for live tumor spheroids. As a non-toxic chemical and an FDA-approved contrast agent, iodixanol is likely to play an important part in the live imaging of deep tissues.

While utilizing the clearing agent may temporarily alter the environment for imaging purposes, we believe this represents a reasonable trade-off, as it allows for high-quality images to be obtained from deep tissues. The reversibility, coupled with the maintenance of cell viability, demonstrates the potential value of this clearing method as a minimally invasive and non-toxic tool for live spheroid imaging. Additionally, while image denoising algorithms can improve the quality of noisy images to some extent, they cannot fully eradicate the noise and artifacts attributed to light scattering and absorption in spheroids. As such, combining the clearing method with imaging processing algorithms to enhance the signal-to-noise ratio and contrast of images may prove more effective and reliable than relying solely on image processing techniques.

Current tissue clearing methods have been previously combined with the microfluidic platform for on-chip clearing of 3D cell cultures. For instance, Chen et al. engineered a microfluidic system to load 3D micro-tissues via gravity and to rapidly render intact micro-tissues optically transparent by inducing pressure-driven flow [12]. Grist et al. have also demonstrated a microfluidic platform for high-throughput clearing of breast cancer spheroids to address the issue of handling difficulty [34]. Santisteban et al. integrated the CLARITY method on a chip and decreased the clearing

Biomedical Optics EXPRESS

time of hydrogel-embedded tissues by using an osmotic pump mechanism [36]. In addition, Oh et al. have combined tissue optical clearing with a minipillar array chip for high-content phenotypic analysis of microtumors [37]. To achieve on-chip 3D imaging, Zhang et al. combined a simplified CLARITY method with lens-free holographic on-chip microscopy [35]. There is no doubt that the integration of tissue clearing methods with microfluidic devices has enabled high-throughput imaging of 3D cell cultures, but is still limited to fixed tissues. Compared to these chip designs, the microfluidic device in our study integrated 3D culture, clearing and live imaging on a chip, which has not been reported previously. This design is expected to facilitate dynamic monitoring of the growth, development, and pathological reactions in 3D cell cultures.

There are many methods that can be used to form spheroids, including low adherent surface, matrix-embedded, hanging drop, and droplet-based spheroids [46]. In this work, the U-shaped bottom low-adherent surface was chosen because it is convenient, and easy to use with uniform-sized spheroids, and the spheroids can be cultured long-term due to the presence of PDMS [47].Generally, the spheroids are subjected to shear stress through flow [46], the design of parallel channels combined with micropillars in our device can overcome these problems to a certain degree.

PDMS surface modification has been popular for microfluidic devices in cell culture [48]. Low adherence is required to facilitate spheroid formation, while some adherence is needed to catch the spheroid prior to clearing and imaging. These two requirements for surface treatment are contradictory, making it hard to achieve them in the same device. In our study, we noticed that the L-polylysine-treated adherence surface was more robust to harsh conditions during fabrication than the low adherence surface. With this feature, we completed the adherence treatment of the cover glass prior to device fabrication, followed by low adherence treatment of the intact device, which would not destroy the adherence surface. Accordingly, the differentiated surface treatment and the hydrophilic difference between the cover glass and the PDMS chambers make it possible to culture and image spheroids on the same device.

Lysosomes are widely known to participate in a variety of cellular activities. They not only play the role of 'garbage disposal,' but emerging evidence suggests that they are involved in other processes such as cell adhesion/migration, apoptosis, and metabolic signal transduction, which are all closely related to cancer development and progression [49]. Previous studies have shown that lysosomes undergo dynamic changes in quantity, morphology, and motility in cancer progression [49–51]. Our investigation reveals that lysosome motility varies across different depths of the sample, even small differences in depth can result in noticeable changes, as evidenced in Fig. 4(e). The motility difference we observed in different layers might be attributed to the gradient of oxygen or carbon dioxide, as well as nutrient content in 3D spheroids. We speculate that the reason more active lysosomes are observed in the deep layer is that cancer cells in this location require increased lysosome motility for sufficient nutrients to support cell growth or proliferation [49,50]. Previous studies have reported that spheroids possess a heterogeneous structure and function, with different regions exhibiting varied levels of oxygenation, nutrient availability, proliferation, differentiation, and apoptosis [52]. It is thus reasonable to expect that lysosomes in different regions of spheroids would demonstrate distinct motility patterns. Thus increasing the imaging depth by just tens of micrometers can yield critical insights into cell activities. The microfluidic-based on-chip culture, clearing, and live imaging pipeline permits the dynamic monitoring of lysosome motility in deep tissues and might facilitate the comprehensive examination of specific lysosome changes in cancer, thereby providing more opportunities for cancer diagnosis and targeted lysosomal treatment [49].

Similarly to real tumors, 3D tumor spheroids exhibit variations in cell states with depth due to the nutrient gradient. Nevertheless, live imaging of deep cells in tumor spheroids remains challenging. Our study showed that using 20% v/v iodixanol solution as a clearing agent for live 3D cell cultures like tumor spheroids can significantly improve the imaging depth and resolution,

Biomedical Optics EXPRESS

thereby permitting the observation of more information, such as cell numbers and lysosome movement. These changes may indicate the metabolic and stress responses of cells during tumor development, and thus, hold significance for studying the physiological and pathological states of cells. We are convinced that this clearing method can provide a new tool for dynamically monitoring live 3D cell cultures, and aid in revealing the behavior and mechanism of cells under different conditions.

There are also some limitations of this clearing method. Firstly, the on-chip pipeline requires the attachment of spheroids to cover glass. Although a study involving adhered spheres was conducted to investigate liver organoids, with no significant effects of attachment on cell behavior found [53], the impact of attachment on spheroid morphology still requires clarification. Exploring alternative techniques for holding spheroids without attachment, such as using hydrogels, might solve the issue. Secondly, to capture images over prolonged periods (hours or days), it may be necessary to optimize the clearing reagent further, while taking safety factors into account. Thirdly, the clearing method can be combined with image processing algorithms in future work, including deep learning-based methods, potentially enhancing image quality and information extraction. Fourthly, this on-chip clearing method is primarily suitable for small-scale 3D cell cultures with a diameter of below 1000 μm, and it may not be valid for larger or more complicated organoids that require extended clearing times and higher clearing efficiency.

As a representative 3D culture model, we used tumor spheroids to demonstrate the feasibility of this on-chip clearing platform. We expect this platform to be extended to other 3D cell cultures, such as monitoring neuronal network activities in brain organoids, and tracking calcium signals in cardiac organoids.

5. Conclusion

In this study, we developed an on-chip clearing method for live imaging of 3D cell cultures on a microfluidic platform. This method increased the imaging performance with good fluorescence compatibility and safety, enabling monitoring of the dynamic movement of lysosomes in deep 3D cell cultures. The combination of the 'organ-on-a-chip' and tissue optical clearing technique is expected to provide an important tool for dynamic tracking of growth, development, and pathological reactions of 3D cell cultures on a chip, and has great potential in biological research and drug discovery.

Funding. National Key Research and Development Program of China (2017YFA0700501); Innovation Fund of WNLO.

Acknowledgments. We thank Prof. Yiwei Li from HUST for providing the MCF-7 cell line, Prof. Shangbang Gao from HUST for providing osmometer, Prof. Weihua Chen for providing viscometer. We also thank the Optical Bio-imaging Core Facility of WNLO-HUST for their assistance with data acquisition.

Disclosures. The authors declare no conflicts of interest.

Data availability. Data underlying the results presented in this paper are not publicly available at this time but may be obtained from the authors upon reasonable request.

Supplemental document. See Supplement 1 for supporting content.

References

1. F. Pampaloni, E. G. Reynaud, and E. H. Stelzer, "The third dimension bridges the gap between cell culture and live tissue," Nat. Rev. Mol. Cell Biol. **8**(10), 839–845 (2007).
2. D. E. Ingber, "Is it time for reviewer 3 to request human organ chip experiments instead of animal validation studies?" Adv. Sci. **7**(22), 2002030 (2020).
3. Y. Wang and H. Jeon, "3D cell cultures toward quantitative high-throughput drug screening," Trends Pharmacol. Sci. **43**(7), 569–581 (2022).
4. L. Venkataraman, S. R. Fair, C. A. McElroy, M. E. Hester, and H. Fu, "Modeling neurodegenerative diseases with cerebral organoids and other three-dimensional culture systems: focus on Alzheimer's disease," Stem Cell Rev. Rep. **18**(2), 696–717 (2022).

Biomedical Optics EXPRESS

5. J. Kim, B. K. Koo, and J. A. Knoblich, "Human organoids: model systems for human biology and medicine," Nat. Rev. Mol. Cell Biol. **21**(10), 571–584 (2020).
6. H. N. Kim, N. L. Habbit, C. Y. Su, N. Choi, E. H. Ahn, E. A. Lipke, and D. H. Kim, "Microphysiological systems as enabling tools for modeling complexity in the tumor microenvironment and accelerating cancer drug development," Adv. Funct. Mater. **29**(22), 1807553 (2019).
7. H. Xu, X. Lyu, M. Yi, W. Zhao, Y. Song, and K. Wu, "Organoid technology and applications in cancer research," J. Hematol. Oncol. **11**(1), 116 (2018).
8. D. Huh, G. A. Hamilton, and D. E. Ingber, "From 3D cell culture to organs-on-chips," Trends Cell Biol. **21**(12), 745–754 (2011).
9. P. Järvinen, A. Bonabi, V. Jokinen, and T. Sikanen, "Simultaneous culturing of cell monolayers and spheroids on a single microfluidic device for bridging the gap between 2D and 3D cell assays in drug research," Adv. Funct. Mater. **30**(19), 2000479 (2020).
10. B. Xiong, K. Ren, Y. Shu, Y. Chen, B. Shen, and H. Wu, "Recent developments in microfluidics for cell studies," Adv. Mater. **26**(31), 5525–5532 (2014).
11. I. R. Suhito and T.-H. Kim, "Recent advances and challenges in organoid-on-a-chip technology," Organoid **2**, e4 (2022).
12. Y. Y. Chen, P. N. Silva, A. M. Syed, S. Sindhwani, J. V. Rocheleau, and W. C. Chan, "Clarifying intact 3D tissues on a microfluidic chip for high-throughput structural analysis," Proc. Natl. Acad. Sci. U. S. A. **113**(52), 14915–14920 (2016).
13. K. Moshksayan, N. Kashaninejad, M. E. Warkiani, J. G. Lock, H. Moghadas, B. Firoozabadi, M. S. Saidi, and N.-T. Nguyen, "Spheroids-on-a-chip: Recent advances and design considerations in microfluidic platforms for spheroid formation and culture," Sens. Actuators, B **263**, 151–176 (2018).
14. E. Leary, C. Rhee, B. T. Wilks, and J. R. Morgan, "Quantitative live-cell confocal imaging of 3D spheroids in a high-throughput format," SLAS Technol. **23**(3), 231–242 (2018).
15. B. N. Ondatje, S. Sances, M. J. Workman, and C. N. Svendsen, "Tissue clearing of human iPSC-derived organ-chips enables high resolution imaging and analysis," Lab Chip **22**(21), 4246–4255 (2022).
16. D. S. Richardson, W. Guan, K. Matsumoto, C. Pan, K. Chung, A. Erturk, H. R. Ueda, and J. W. Lichtman, "Tissue clearing," Nat. Rev. Methods Primers **1**(1), 84 (2021).
17. K. Tainaka, A. Kuno, S. I. Kubota, T. Murakami, and H. R. Ueda, "Chemical principles in tissue clearing and staining protocols for whole-body cell profiling," Annu. Rev. Cell Dev. Biol. **32**(1), 713–741 (2016).
18. T. Yu, J. Zhu, D. Li, and D. Zhu, "Physical and chemical mechanisms of tissue optical clearing," iScience **24**(3), 102178 (2021).
19. E. A. Susaki and H. R. Ueda, "Whole-body and whole-organ clearing and imaging techniques with single-cell resolution: toward organism-level systems biology in mammals," Cell Chem. Biol. **23**(1), 137–157 (2016).
20. D. Zhu, K. V. Larin, Q. Luo, and V. V. Tuchin, "Recent progress in tissue optical clearing," Laser. Photonics. Rev. **7**(5), 732–757 (2013).
21. V. V. Tuchin, I. L. Maksimova, D. A. Zimnyakov, I. L. Kon, A. H. Mavlyutov, and A. Mishin, "Light propagation in tissues with controlled optical properties," J. Biomed. Opt. **2**(4), 401–417 (1997).
22. V. V. Tuchin, *Optical Clearing of Tissues and Blood* (SPIE Press, 2006).
23. V. V. Tuchin, D. Zhu, and E. A. Genina, *Handbook of Tissue Optical Clearing: New Prospects in Optical Imaging* (CRC Press, 2022).
24. E. A. Susaki and M. Takasato, "Perspective: extending the utility of three-dimensional organoids by tissue clearing technologies," Front. Cell Dev. Biol. **9**, 679226 (2021).
25. E. Nurnberg, M. Vitacolonna, J. Klicks, E. von Molitor, T. Cesetti, F. Keller, R. Bruch, T. Ertongur-Fauth, K. Riedel, P. Scholz, T. Lau, R. Schneider, J. Meier, M. Hafner, and R. Rudolf, "Routine optical clearing of 3D-cell cultures: simplicity forward," Front. Mol. Biosci. **7**, 20 (2020).
26. E. C. Costa, D. N. Silva, A. F. Moreira, and I. J. Correia, "Optical clearing methods: an overview of the techniques used for the imaging of 3D spheroids," Biotechnol. Bioeng. **116**(10), 2742–2763 (2019).
27. Y. Miura, M. Y. Li, O. Revah, S. J. Yoon, G. Narazaki, and S. P. Pasca, "Engineering brain assembloids to interrogate human neural circuits," Nat. Protoc. **17**(1), 15–35 (2022).
28. A. Albanese, J. M. Swaney, D. H. Yun, N. B. Evans, J. M. Antonucci, S. Velasco, C. H. Sohn, P. Arlotta, L. Gehrke, and K. Chung, "Multiscale 3D phenotyping of human cerebral organoids," Sci. Rep. **10**(1), 21487 (2020).
29. M. E. Boutin and D. Hoffman-Kim, "Application and assessment of optical clearing methods for imaging of tissue-engineered neural stem cell spheres," Tissue Eng., Part C **21**(3), 292–302 (2015).
30. E. C. Costa, A. F. Moreira, D. de Melo-Diogo, and I. J. Correia, "Polyethylene glycol molecular weight influences the Clear^{T2} optical clearing method for spheroids imaging by confocal laser scanning microscopy," J. Biomed. Opt. **23**(05), 1 (2018).
31. D. N. Silva, E. C. Costa, C. F. Rodrigues, D. de Melo-Diogo, I. J. Correia, and A. F. Moreira, "Influence of ClearT and ClearT2 agitation conditions in the fluorescence imaging of 3D spheroids," Int. J. Mol. Sci. **22**(1), 266 (2020).
32. L. Lallemant, C. Lebreton, and M. Garfa-Traore, "Comparison of different clearing and acquisition methods for 3D imaging of murine intestinal organoids," J. Biol. Methods **7**(4), e141 (2020).
33. E. Steinberg, N. Orehov, K. Tischenko, O. Schwob, G. Zamir, A. Hubert, Z. Manevitch, and O. Benny, "Rapid clearing for high resolution 3D imaging of ex vivo pancreatic cancer spheroids," Int. J. Mol. Sci. **21**(20), 7703 (2020).

Biomedical Optics EXPRESS

34. S. M. Grist, S. S. Nasseri, T. Poon, C. Roskelley, and K. C. Cheung, "On-chip clearing of arrays of 3-D cell cultures and micro-tissues," Biomicrofluidics **10**(4), 044107 (2016).
35. Y. B. Zhang, Y. Shin, K. Sung, S. Yang, H. Chen, H. D. Wang, D. Teng, Y. Rivenson, R. P. Kulkarni, and A. Ozcan, "3D imaging of optically cleared tissue using a simplified CLARITY method and on-chip microscopy," Sci. Adv. **3**(8), e1700553 (2017).
36. T. Silva Santisteban, O. Rabajania, I. Kalinina, S. Robinson, and M. Meier, "Rapid spheroid clearing on a microfluidic chip," Lab Chip **18**(1), 153–161 (2018).
37. M. S. Oh, I. A. Khawar, D. W. Lee, J. K. Park, and H. J. Kuh, "Three-dimensional imaging for multiplex phenotypic analysis of pancreatic microtumors grown on a minipillar array chip," Cancers **12**(12), 3662 (2020).
38. K. Dabov, A. Foi, V. Katkovnik, and K. Egiazarian, "Image denoising by sparse 3-D transform-domain collaborative filtering," IEEE Trans. Image Process. **16**(8), 2080–2095 (2007).
39. J. Wang, R. Shi, and D. Zhu, "Switchable skin window induced by optical clearing method for dermal blood flow imaging," J. Biomed. Opt. **18**(6), 061209 (2012).
40. C. Zhang, W. Feng, Y. Zhao, T. Yu, P. Li, T. Xu, Q. Luo, and D. Zhu, "A large, switchable optical clearing skull window for cerebrovascular imaging," Theranostics **8**(10), 2696–2708 (2018).
41. Y. Zhao, T. Yu, C. Zhang, Z. Li, Q. Luo, T. Xu, and D. Zhu, "Skull optical clearing window for in vivo imaging of the mouse cortex at synaptic resolution," Light: Sci. Appl. **7**(2), 17153 (2017).
42. D. Li, Z. Hu, H. Zhang, Q. Yang, L. Zhu, Y. Liu, T. Yu, J. Zhu, J. Wu, J. He, P. Fei, W. Xi, J. Qian, and D. Zhu, "A Through-Intact-Skull (TIS) chronic window technique for cortical structure and function observation in mice," eLight **2**(1), 15 (2022).
43. C. Zhang, C. J. Liu, and W. Feng, "A long-term clearing cranial window for longitudinal imaging of cortical and calvarial ischemic injury through the intact skull," Adv. Sci. **9**, 2105893 (2022).
44. T. Boothe, L. Hilbert, M. Heide, L. Berninger, W. B. Huttner, V. Zaburdaev, N. L. Vastenhouw, E. W. Myers, D. N. Drechsel, and J. C. Rink, "A tunable refractive index matching medium for live imaging cells, tissues and model organisms," eLife **6**, 27240 (2017).
45. W. Wu, S. He, J. Wu, C. Chen, X. Li, K. Liu, and J. Y. Qu, "Long-term in vivo imaging of mouse spinal cord through an optically cleared intervertebral window," Nat. Commun. **13**(1), 1959 (2022).
46. M. Khot, M. Levenstein, N. Kapur, and D. Jayne, "A review on the recent advancement in "tumour spheroids-on-a-chip"," J. Cancer Res. Pract. **6**(2), 55 (2019).
47. T. Anada, J. Fukuda, Y. Sai, and O. Suzuki, "An oxygen-permeable spheroid culture system for the prevention of central hypoxia and necrosis of spheroids," Biomaterials **33**(33), 8430–8441 (2012).
48. J. Zhou, A. V. Ellis, and N. H. Voelcker, "Recent developments in PDMS surface modification for microfluidic devices," Electrophoresis **31**(1), 2–16 (2010).
49. T. Tang, Z. Y. Yang, D. Wang, X. Y. Yang, J. Wang, L. Li, Q. Wen, L. Gao, X. W. Bian, and S. C. Yu, "The role of lysosomes in cancer development and progression," Cell Biosci. **10**(1), 131 (2020).
50. J. E. Oyarzun, J. Lagos, M. C. Vazquez, C. Valls, C. De la Fuente, M. I. Yuseff, A. R. Alvarez, and S. Zanlungo, "Lysosome motility and distribution: relevance in health and disease," Biochim. Biophys. Acta Mol. Basis. Dis. **1865**(6), 1076–1087 (2019).
51. S. Piao and R. K. Amaravadi, "Targeting the lysosome in cancer," Ann. N. Y. Acad. Sci. **1371**(1), 45–54 (2016).
52. S. C. Brüningk, I. Rivens, C. Box, U. Oelfke, and G. Ter Haar, "3D tumour spheroids for the prediction of the effects of radiation and hyperthermia treatments," Sci. Rep. **10**(1), 1653 (2020).
53. X. Xu, S. Jiang, L. Gu, B. Li, F. Xu, C. Li, and P. Chen, "High-throughput bioengineering of homogenous and functional human-induced pluripotent stem cells-derived liver organoids via micropatterning technique," Front. Bioeng. Biotechnol. **10**, 937595 (2022).